Journal of Catalysis 264 (2009) 54–66

Contents lists available at ScienceDirect

Journal of Catalysis

journal homepage: www.elsevier.com/locate/jcat

Functional assessment of the strength of solid acid catalysts

Josef Macht, Robert T. Carr, Enrique Iglesia *

Department of Chemical Engineering, University of California at Berkeley, Berkeley, CA 94720, United States

ARTICLE INFO

Article history:
Received 13 December 2008
Revised 24 February 2009
Accepted 8 March 2009
Available online 22 April 2009

Keywords:
Keggin polyoxometalates
2-Butanol dehydration
n-Hexane isomerization
Sulfated zirconia
Tunstated zirconia
Perfluorosulfonic acid resins
Deprotonation energy

ABSTRACT

We describe here a rigorous method to estimate the deprotonation energy (DPE) and acid strength for solid Brønsted acids with uncertain structure using rate constants for reactions involving cationic transition states. The approach exploits relations between turnover rates for dehydration and isomerization reactions and DPE values on Keggin polyoxometalates and H-BEA solids with known structures. These relations are used to estimate the strength of acid sites in SO_4–ZrO_2(SZr), WO_x–ZrO_2(WZr), and perfluorosulfonic resins (SAR) from their alkanol dehydration and alkane isomerization rate constants. Alkanol dehydration and alkane isomerization proceed via pathways independent of acid identity and are limited by steps involving late transition states. Turnover rates (per accessible acid sites measured by titration during catalysis) are related to the relevant rate constants and are used to estimate DPE values for SZr, WZr, and SAR. Isomerization data estimate DPE values of 1110 kJ mol^{-1} and 1120 kJ mol^{-1} for SZr and WZr, respectively, while dehydration rate data lead to slightly higher values (1165 kJ mol^{-1} and 1185 kJ mol^{-1}). The DPE value for SAR was 1154 kJ mol^{-1} from dehydration reactions, but diffusional constraints during reactions of non-polar alkanes precluded isomerization rate measurements. SZr and SAR contain stronger acid sites than zeolites (1185 kJ mol^{-1}), but weaker than those in $H_3PW_{12}O_{40}$ and $H_4SiW_{12}O_{40}$ (1087 kJ mol^{-1} and 1105 kJ mol^{-1}). Acid sites present in WZr during alkane isomerization are stronger than those present in zeolites, but these become similar in strength in the polar environment prevalent during dehydration catalysis. These effects of reaction media (and treatment protocols) reflect differences in the extent of dehydroxylation of catalytic surfaces. OH groups remaining after dehydroxylation are stronger acid sites because of a concomitant decrease in electron density in the conjugate anion and the formation of Brønsted–Lewis acid conjugate pairs. The method proposed and used here probes acid strength (as DPE) on sites of uncertain structure and within solvating media inherent in their use as catalysts. It can be used for any Brønsted acid or reaction, but requires reactivity-DPE relations for acids of known structure, the mechanistic interpretations of rates, and the measurement of accessible protons during catalysis. The resulting DPE values provide a rigorous benchmark for the structural fidelity of sites proposed for acids with uncertain structure, a method to assess the consequences of the dynamic nature of active sites in acid catalysis, and a connection between theory and experiment previously unavailable.

1. Introduction

The catalytic properties of solid Brønsted acids have often been attributed to the strength of their acid sites [1]. Yet, methods required for the rigorous assessment of acid strength have remained elusive. For H-form zeolites, correlations between acid strength and the shifts in O–H stretching frequencies or ^{1}H-lines upon adsorption of basic molecules (by infrared [2–4] and nuclear magnetic resonance [5–7] spectroscopies, respectively) have been proposed. These methods lack, however, a rigorous connection to a specific value of deprotonation energies accessible to theoretical treatments. Also, they cannot assess acid strength within solvating environments relevant to catalytic reactions or provide direct measures of the accessibility, number, or strength of acid sites during catalysis. These approaches are often limited by the broad nature of infrared O–H bands in non-zeolitic acids of catalytic interest, such as Keggin-type polyoxometalate (POM) clusters [8] ($H_3PW_{12}O_{40}$) and perfluorosulfonic acid resins [3,9], restricting, as a result, their current ability to contrast the acid properties among the broad range of useful solid acid catalysts.

The use of adsorption enthalpies for basic molecules, accessible by temperature-programmed desorption or calorimetry, to measure acid strengths is not unambiguous. The assessment of desorption dynamics requires kinetic analyses inadequate for non-uniform ensembles of acid sites [10]; it also requires probe molecules that desorb before they or the solid acid decompose, a ubiquitous problem for Keggin-type POM clusters [11], sulfonic

* Corresponding author. Fax: +1 510 642 4778.
E-mail address: iglesia@berkeley.edu (E. Iglesia).

0021-9517/$ - see front matter © 2009 Elsevier Inc. All rights reserved.
doi:10.1016/j.jcat.2009.03.005

acid resins, and sulfated oxides. Significant contributions to adsorption enthalpies from non-specific van der Waals interactions, especially for molecules confined within zeolites, and specific charge-transfer interactions via hydrogen bonding, which are ubiquitous for adsorbed molecules but not for cationic species at transition states, cause adsorption enthalpies to depend only in part on acid strength.

Acid strength rigorously reflects the energy required to remove a proton from a solid acid; this deprotonation energy (DPE) is a probe-independent intrinsic property of an acid [12]. The ubiquitous involvement of cationic transition states and the more neutral character of adsorbed intermediates (relative to transition states) in solid acids make it essential that we discern the respective and often independent roles of DPE and of specific and non-specific interactions in the stabilization of adsorbed reactants and products and especially of ion-pairs at transition states, which depend on the combined effects of van der Waals, hydrogen-bonding, and electrostatic interactions for stabilization.

We propose here a method for assessing acid strength (as specific DPE values) from the dynamics of any reaction for which mechanistic interpretations implicate kinetically-relevant elementary steps catalyzed by Brønsted acid sites. Our strategy involves turnover rate and selectivity measurements on solid acids of known structure, such as zeolites and POM clusters, for which DPE values can be estimated accurately, under conditions of strict kinetic control [12–14]. The resulting relations are then used to estimate DPE values for solid acids with uncertain or non-uniform site structures at conditions prevalent during each catalytic reaction. Our recent studies have established the rigor and accuracy of such relations for alkanol dehydration and (bifunctional) alkane isomerization on acid forms of Keggin-type POM clusters and zeolites, which are used as solid acids with known structure [12,13].

Brønsted acid sites stabilize cationic transition states formed via protonation of either reactants or reactant-derived intermediates. Quantum chemical methods [13,15–18], the strong effects of carbenium ion stability on reaction barriers and rate constants [12], and the small kinetic isotope effects observed [12] indicate that proton transfer is typically complete at the transition state, which can therefore be accurately treated as an ion pair. As a result, activation barriers (E_a) for elementary steps in acid catalysis depend on the deprotonation energy of the catalyst (DPE), on the reactant or product proton affinities (PA), on the ion-pair interaction energies (ΔE_{int}), and on the enthalpy of adsorption of gas-phase reactants to form bound intermediates preceding the transition state (ΔH_{ads}) (Scheme 1).

The types and properties of acid sites determine transition state energies through the magnitudes of DPE, ΔE_{int}, and ΔH_{ads}, indicating that activation barriers depend on the ability of an acid to donate a proton (DPE), but also on its role in stabilizing the reactants (ΔH_{ads}) and the cationic species in the ion-pair (ΔE_{int}), for the latter predominantly via electrostatic interactions. The extent to which DPE values are compensated by ΔE_{int} defines the energy relevant to the stability of the transition state and thus to catalytic reactivity [12]; yet, these are not available from characterization methods that exploit the binding of probe molecules, often stabilized via covalent or van der Waals interactions, within environments extraneous to catalysis. The contributions from ΔH_{ads} to the relevant activation barriers depend on whether adsorbed reactants are present as hydrogen-bonded alkanols [12,14] or as covalently bound alkoxides [19]. Differences in ΔH_{ads} values among various acids in 2-butanol dehydration [14] and *n*-hexane isomerization [19] were, however, much smaller than the differences among the respective transition state energies. Therefore, the range of barriers and rate constants for an elementary step on solid acids is predominantly determined by the catalyst DPE and by its ability to stabilize the transition state by electrostatic interactions as an ion-pair.

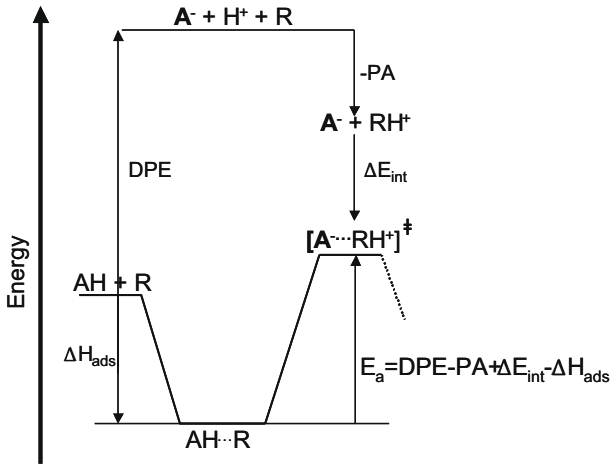

Scheme 1. Thermochemical cycle for acid–base reactions on Brønsted acid catalysts. The activation barrier (E_a) is determined by the deprotonation energy (DPE) of the acid (AH), the "proton affinity" (PA), the ion-pair stabilization energy (ΔE_{int}), and the reactant adsorption energy (ΔH_{ads}).

Alkanol dehydration and bifunctional *n*-hexane isomerization are used here as specific probe reactions, but the strategy described and implemented is general for chemical reactions with kinetically-relevant elementary steps catalyzed by Brønsted acids, as long as rate measurements can be interpreted rigorously in terms of kinetic and/or thermodynamic parameters for *elementary* steps and the number of accessible protons is measured during catalysis. Elimination and isomerization elementary steps and their kinetic-relevance are well understood [12,14,19–21] and allow rates and selectivities to be interpreted as rate and equilibrium constants and consequently in terms of the stability of adsorbed species and cationic transition states. As a result, the effects of DPE and ΔE_{int} can be rigorously assessed for materials with well-defined structures, which are amenable to quantum chemical calculations. We have recently reported accurate and rigorous connections between rate (and equilibrium) constants and DPE for elementary steps in dehydration and isomerization reactions on acid zeolites and POM clusters [12,14,19]. These studies showed that DPE and transition state stabilization energies determine activation barriers and that rate constants decrease exponentially with increasing DPE values.

Sulfated zirconia (SZr) [22–25], WO_x domains supported on zirconia (WZr) [26–28], and perfluorosulfonic acid resins (SAR; e.g. Nafion®) [29] catalyze some chemical reactions more effectively than acidic zeolites. Here, we probe the acid properties of these solid acids, for which structures are uncertain and DPE estimates, which depend on the structures assumed in calculations, are unreliable. We show that the mechanisms involved in Keggin POM and H-BEA catalysts also apply to SZr, WZr, and SAR for alkanol dehydration (Section 3.1) and for SZr and WZr for bifunctional alkane isomerization (Section 3.4). We also report measurements of acid site densities *during* catalysis using titration with 2,6-di-*tert*-butylpyridine on these materials (Sections 3.2 and 3.5) and use them to measure their intrinsic site reactivity in terms of turnover rates. The number of accessible Brønsted acid sites in SZr and WZr depends on treatment and reaction conditions, specifically on temperature, H_2O concentration (on SZr) [30], and reductant and oxidant concentrations and identity (on WZr) [31]. The relations between reactivity and DPE developed for well-defined acids are then used here to provide DPE estimates for SZr, WZr, and SAR catalysts with unknown active site structure (Sections 3.3 and 3.6). These DPE estimates can then be used to benchmark the fidelity of the various acid site structures considered for SO_4–ZrO_2 and

WO_x–ZrO_2 catalysts (Section 3.7). For these materials, the number and strength of acid sites, therefore, do not depend solely on the composition or initial structure of solids, but also on solvation effects during catalysis and on their thermal history during treatments.

2. Experimental and theoretical methods

2.1. Catalyst synthesis and characterization

Synthesis protocols for SZr [32], WZr [31], and SAR [29] have been reported earlier. Sulfated zirconium hydroxide (Magnesium Electron, Inc. (XZO 1077/01)) was heated in static ambient air (0.17 K s^{-1}, 3 h, 873 K); the resulting material had a N_2 BET surface area of 109 $m^2\,g^{-1}$ and 0.44 (mmol sulfate) g^{-1} [32]. WZr was prepared by aqueous impregnation of zirconium oxyhydroxide, precipitated from a 0.5 M aqueous solution of zirconyl chloride ($ZrOCl_2 \cdot 8H_2O$, Aldrich, >98 wt%) at constant pH (10, controlled using NH_4OH, Aldrich 99%) with the required amount of an aqueous ammonium metatungstate solution ($(NH_4)_6H_2W_{12}O_{40}$, Strem Chemicals, 99.9%) to give a material containing 15 wt% of WO_3 [31]. The impregnated WZr powders were dried at 383 K and treated in flowing dry air (Matheson, zero grade, 1 $cm^3\,s^{-1}\,g^{-1}$) at 1023 K; its N_2 BET surface area was 49 $m^2\,g^{-1}$ and the WO_x surface density was 7.9 nm^{-2}. The Nafion®-SAC13 material was used as received (Sigma–Aldrich) and is denoted as SAR. A surface area of 350 $m^2\,g^{-1}$ and a concentration of Brønsted acid sites of 0.14 mmol g^{-1} have been reported for this material [33]. Physical mixtures of SZr, SAR, and WZr with Pt/Al_2O_3 (Pt/Al_2O_3 prepared as reported [19]) were prepared by mixing and grinding the metal and acid co-catalysts into small aggregates ($Pt/H^+ = 1$; <10 μm diameter). These mixtures were pressed into wafers, crushed, and sieved to retain 125–180 μm aggregates; they were used as bifunctional catalysts in alkane isomerization studies.

2.2. n-Hexane isomerization catalysis

Isomerization rates and selectivities were measured at 473 K in a tubular quartz flow reactor (1.0 cm inner diameter; 0.1–0.3 g catalysts). SAR and WZr samples were held onto a porous quartz disc and heated to 473 K at 0.083 K s^{-1} in flowing He (0.83 $cm^3\,s^{-1}$) before rate measurements. SZr catalysts were treated at 673 K in He (0.83 $cm^3\,g^{-1}\,s^{-1}$) for 2 h before *n*-hexane isomerization reactions. Sample temperatures were measured using a K-type thermocouple located within a dimple in the external quartz wall of the reactor and were controlled (±0.2 K) using a Watlow controller (Series 982) and a resistively heated furnace. Transfer lines were held at 393 K to prevent adsorption or condensation of reactants, products, or titrants. *n*-Hexane reactants (Sigma–Aldrich, 99%, Fluka, 99%) were used without additional purification and were introduced as a liquid using a syringe pump (Cole Parmer, 74900 series) by vaporization into a He (Praxair, UHP) and H_2 (Praxair, UHP) stream at 393 K. Molar flow rates of He, H_2 and *n*-hexane were controlled independently to give the desired reactant molar ratios (*n*-hexane/H_2 = 0.05–1) and space velocities and to maintain low and relatively constant *n*-hexane conversions (1–6%). Reactant and product concentrations were measured by gas chromatography using flame ionization detection (Agilent 6890N GC, 50 m HP-1 column, methyl silicone, 50 m × 0.32 mm × 1.05 μm). Brønsted acid sites were titrated by introducing 2,6-di-*tert*-butylpyridine (Aldrich, 97%) dissolved in the *n*-hexane reactants into He/H_2 streams at 393 K. The amount of titrant adsorbed on the catalyst was measured from its residual concentration in the effluent stream using the same chromatographic protocols as for catalytic reactions.

2.3. 2-Butanol dehydration catalysis

Rates and selectivities were measured at 343 K in a quartz flow cell (1.0 cm inner diameter; 0.02–0.2 g catalyst; 125–180 μm aggregates) using protocols similar to those for *n*-hexane isomerization. 2-Butanol reactants (Sigma–Aldrich, 99.5%) were used without purification and introduced as a liquid using a syringe pump (Cole Parmer, 74900 series) by vaporization into flowing He (Praxair, UHP) at 393 K. Molar rates of He and of all gaseous species were adjusted to give the desired reactant pressures and to maintain low and relatively constant reactant conversions (<10%). Only the alkene products of dehydration reactions were detected (1-butene, cis-2-butene, trans-2-butene). Deactivation by oligomerization reactions was not observed at the low alkanol conversions and low alkene concentrations prevalent in these experiments. Brønsted acid sites were titrated by introducing 2,6-di-*tert*-butylpyridine (Aldrich, 97%) dissolved in 2-butanol reactants (Sigma–Aldrich, 99.5%, anhydrous) into flowing He and vaporized at 393 K to give a stream containing 0.5 kPa 2-butanol and 0.9 Pa 2,6-di-*tert*-butylpyridine.

2.4. Theoretical calculations and methods

Density functional calculations were performed using the Gaussian 03 program [34]. Geometries were optimized and energies calculated at the B3LYP/6-31 + G(d,p) level of theory. The DPE values for Keggin-type POM clusters have been reported earlier [14,35].

3. Results and discussion

3.1. Kinetics and mechanism of 2-butanol dehydration on SO_4–ZrO_2, WO_x–ZrO_2 and sulfonic acid resins

2-Butanol dehydration rates decreased with increasing reactant pressure on SZr, WZr, and SAR catalysts (Fig. 1a). Similar dehydration rate dependence on 2-butanol partial pressures on SAR catalysts has previously been reported [52]. This reaction proceeds via elementary steps that include quasi-equilibrated molecular adsorption of 2-butanol on Brønsted acid sites via hydrogen bonding (Step 1, Scheme 2) to form "monomers" [12–14]. These monomers then decompose irreversibly via E1-type pathways, in which C_α—OH_2^+ bonds are cleaved to form water molecules and adsorbed butoxides in kinetically-relevant steps involving carbenium ions at late transition states (Step 2, Scheme 2). The catalytic dehydration cycle is completed by deprotonation of adsorbed butoxides (Step 3, Scheme 2) to form alkenes. Butanol monomers can also interact with another 2-butanol molecule to form unreactive dimers, which are stabilized by hydrogen bonds [–O–H···O–] between the two molecules (Step 4, Scheme 2).

These elementary steps lead to a rate equation that accurately describes all 2-butanol dehydration rate data on Keggin clusters and H-BEA zeolites [12,13]:

$$r = \frac{k_2[H^+]}{1 + K_4[C_4H_9OH]} \quad (1)$$

In this equation, k_2 is the elimination step rate constant (Step 2, Scheme 2) and K_4 is the equilibrium constant for dimer formation (Step 4, Scheme 2); $[H^+]$ represents the number of accessible protons. The form of Eq. (1) reflects the presence of 2-butanol monomers and dimers as most abundant surface species during catalysis. For Keggin-type POM clusters, the proposed elementary steps and their kinetic relevance are consistent with all kinetic and isotopic data and with DFT estimates of activation barriers [12,13]. This rate equation also describes all available 2-butanol

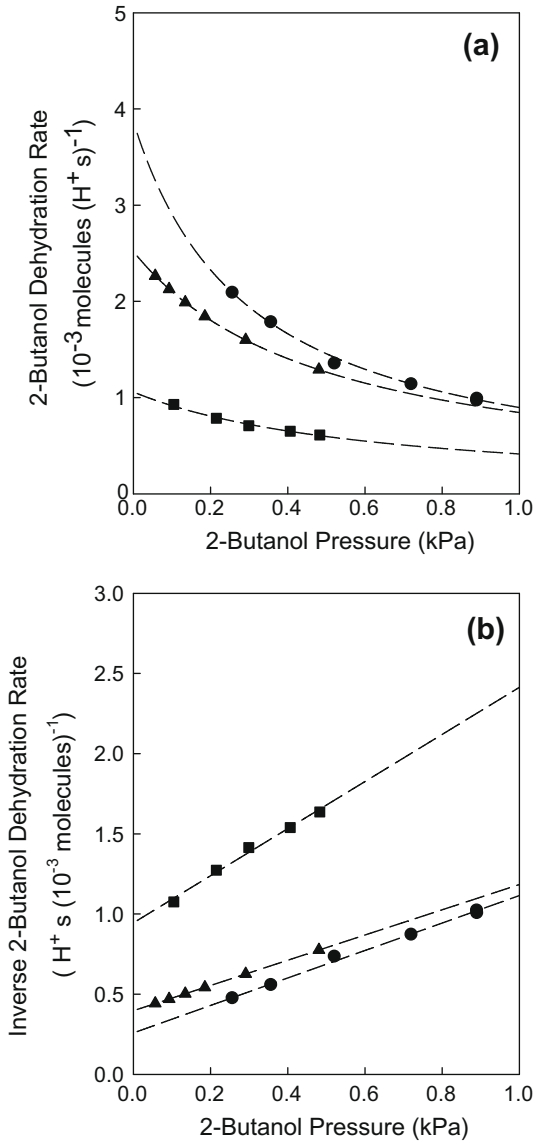

Fig. 1. 2-Butanol dehydration rates (per H^+) (a) and inverse 2-butanol dehydration rates (b) as a function of 2-butanol pressure for SZr (▲), WZr (■), and SAR (●) (343 K, conversion < 10%). Dashed lines represent the predictions from Eq. (1).

dehydration data on H-BEA, as well as the rates of dehydration for other alkanols and ethers on all Keggin-type POM clusters [12].

Fig. 1a shows 2-butanol dehydration rates predicted using values for k_2 and K_4 obtained by regressing rate data to the form of Eq. (1) for each catalyst (dashed curves). The excellent agreement between predicted and measured rates in Fig. 1a shows that Eq. (1) accurately describes 2-butanol dehydration rate data also on SZr, WZr, and SAR. Reciprocal 2-butanol dehydration rates show a linear dependence on 2-butanol pressure (Fig. 1b), as expected from the functional form of Eq. (1) and also as observed on POM clusters and acid zeolites [12].

3.2. Measurement of the number of accessible protons during 2-butanol dehydration by 2,6-di-tert-butylpyridine titration on SO_4–ZrO_2, WO_x–ZrO_2, and sulfonic acid resins

The regression of these kinetic rate data gives values for $k_2[H^+]$ and K_4; therefore intrinsic elimination rate constants (k_2) require independent measurements of the number of protons ($[H^+]$) accessible *during* catalysis. We measure these here by titration with 2,6-di-*tert*-butylpyridine during 2-butanol dehydration; 2,6-di-*tert*-butylpyridine adsorbs to Brønsted acid sites in competition with alkanol reactants, but cannot coordinate to Lewis acid sites because of steric hindrance around its nitrogen atom [36].

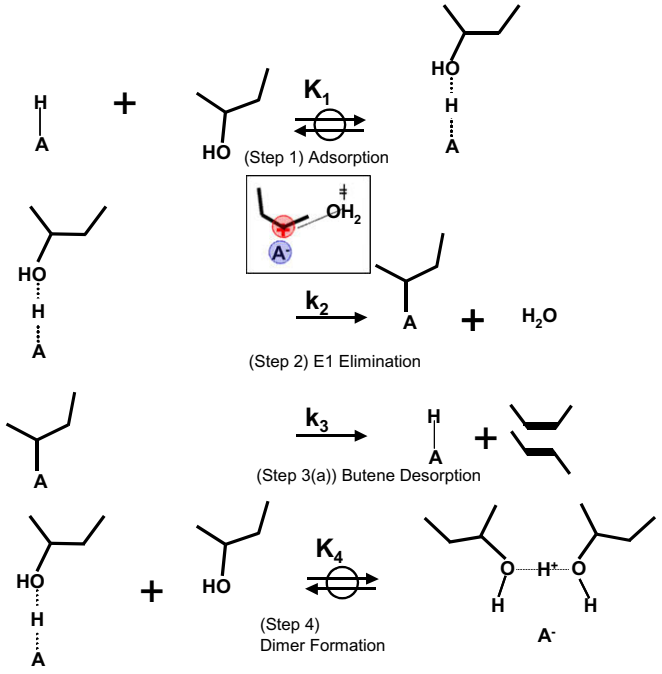

Scheme 2. Proposed sequence of elementary steps for 2-butanol dehydration on Brønsted acid catalysts (HA) [12,13]. The sequence of elementary steps is also applicable to the dehydration reactions of other alkanol reactants and ether cleavage reactions [12].

Fig. 2 shows 2-butanol dehydration rates on SZr as Brønsted acid sites are titrated by 2,6-di-*tert*-butylpyridine. The left panel

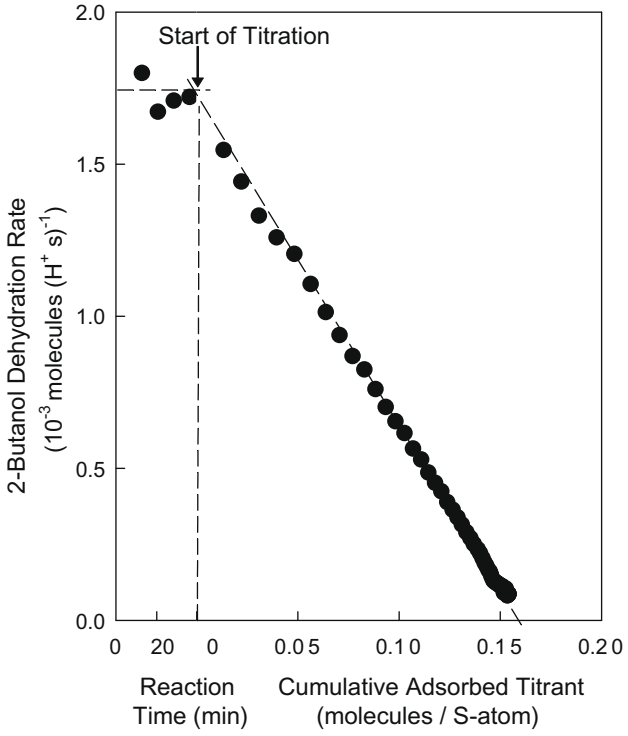

Fig. 2. Titration of acid sites on SZr during 2-butanol dehydration at 343 K. Reaction rates (per H^+) at 343 K as a function of the cumulative amount of titrant (2,6-di-*tert*-butylpyridine) adsorbed (0.2 kPa 2-butanol, 0.9 Pa 2,6-di-*tert*-butylpyridine).

in Fig. 2 shows dehydration rates before adding the titrant, while the right panel shows rates as a function of the amount of titrant adsorbed. 2-Butanol dehydration rates decreased as 2,6-di-*tert*-butylpyridine irreversibly titrates Brønsted acid sites. The titrant uptake required to completely suppress dehydration rates (0.16 (S-atom)$^{-1}$, Fig. 2) provides an upper bound for the number of Brønsted acid sites responsible for measured reaction rates; it is an upper bound because we cannot rule out that sites inactive for catalysis are titrated concurrently and irreversibly. 2-Butanol dehydration rates decreased linearly with 2,6-di-*tert*-butylpyridine uptakes (Fig. 2); these trends do not give unequivocal evidence for acid sites uniform in reactivity or strength, because 2,6-di-*tert*-butylpyridine titrates all acid sites that bind it irreversibly, irrespective of their reactivity, before it titrates sites farther along the bed.

The titration of Brønsted acid sites by 2,6-di-*tert*-butylpyridine led to a linear decrease in dehydration rates and to their complete suppression also on WZr and SAR catalysts. Measured titrant uptakes were 0.06 (W-atom)$^{-1}$ on WZr. The number of accessible protons in WZr depends strongly on WO_x surface density [31]. These titrant uptakes are slightly larger than reported earlier during 2-butanol dehydration at 373 K (~0.04 (W-atom)$^{-1}$) [31] for samples with similar WO_x surface density, possibly because of loss of Brønsted acid sites via hydroxyl recombination at the higher reaction temperatures used in the previous study (373 K vs. 343 K).

The titrant uptake on SAR was one titrant per proton, where the number of protons was determined independently from its Na^+ exchange capacity [33]. The stoichiometric titration of all protons in SAR is surprising because this material consists of agglomerates of the resin (20–60 nm diameter) and SiO_2 particles [29,33]. Thus, some protons may reside within inaccessible regions. The 2,6-di-*tert*-butylpyridine uptakes indicate, however, that these titrants can access protons within the perfluorosulfonic acid resin particles in spite of their large size, at least when polar 2-butanol reactants are also present.

We discuss next how the k_2 values from the 2-butanol dehydration rate data and 2,6-di-*tert*-butylpyridine uptakes can be used to estimate DPE values (and probe acid strength) for SZr, WZr, and SAR catalysts. These DPE values cannot be estimated reliably by theory because of significant uncertainties in the structure of the active acid sites present in these materials.

3.3. Estimates of deprotonation energies from 2-butanol dehydration rate constants on SO_4–ZrO_2, WO_x–ZrO_2, and sulfonic acid resins

Fig. 3 shows 2-butanol dehydration rate constants (with the ordinate as a logarithmic scale) as a function of DPE on Keggin-type POM clusters supported on SiO_2 ($H_{8-n}X^{n+}W_{12}O_{40}$, X = P^{5+}, Si^{4+}, Al^{3+}, Co^{2+}; in order of increasing DPE) and on H-BEA. The well-defined structure and composition of these materials allow reliable DPE estimates using density functional theory (DFT) [12,14]. The line regressed through these 2-butanol dehydration rate constants shows that there is a common exponential dependence of these rate constants on DPE, consistent with thermochemical cycle treatments of elimination elementary steps (Scheme 1), as discussed next.

The effects of DPE on dehydration rate constants and activation barriers are rigorously addressed by thermochemical cycles that describe the stability of cationic transition states in terms of the relevant reactant and catalyst properties [12,37]. The barrier for a reaction step catalyzed by Brønsted acids (E_a) depends on (i) the energy required to deprotonate the acid (DPE), (ii) the energy of corresponding gas-phase reactions of reactants with protons (e.g., ROH + H^+ → R^+ + H_2O for dehydration reactions with late transition states), (iii) the interaction energy of the ion-pair at the transition state, resulting mainly from electrostatic stabilization of the cationic species by the anionic conjugate base (ΔE_{int}), and (iv) the enthalpy of the adsorbed intermediates immediately preceding the transition state (relative to the isolated reactant(s) in the contacting gas phase and the acid) (ΔH_{ads}) according to (Scheme 1):

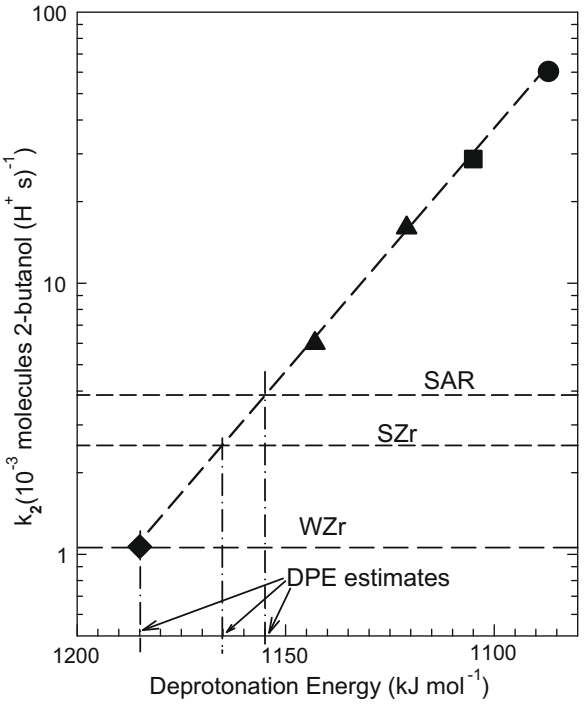

Fig. 3. 2-Butanol dehydration rate constants (k_2) (Scheme 2, Step 2) as a function of deprotonation energy (ΔE_{rxn} for HA → A^- + H^+ (non-interacting), where HA is the acid and A^- is the conjugate base) calculated by DFT for $0.04H_3PW/Si$ (●), $0.04H_4SiW/Si$ (■), $0.04H_5AlW/Si$ (▲), $0.04H_6CoW/Si$ (▼), and H-BEA (◆). Measured 2-butanol dehydration rate constants for SZr, WZr, and SAR are shown as dashed horizontal lines. k_2 values were obtained by fitting Eq. (1) to the kinetic data and normalization by the 2,6-di-*tert*-butylpyridine uptake (see also Table 1), which corresponds to the number of accessible protons.

$$E_a = \mathrm{DPE} - \mathrm{PA} + \Delta E_{int} - \Delta H_{ads} \quad (2)$$

Changes in the central atom in Keggin-type POM clusters increased DPE values by 34 kJ mol^{-1} as its valence decreased (1087 kJ mol^{-1}; $H_3PW_{12}O_{40}$ and 1121 kJ mol^{-1}; $H_5AlW_{12}O_{40}$) [14]. This range of DPE values increased activation barriers (derived from DFT) for 2-butanol dehydration by only 13.4 kJ mol^{-1} because of more effective electrostatic stabilization as DPE values increased [14]. For example, ΔE_{int} values derived from DFT are 318 kJ mol^{-1} for $H_3PW_{12}O_{40}$ and 335 kJ mol^{-1} for $H_5AlW_{12}O_{40}$, a difference of 17 kJ mol^{-1} [14]. Similar compensation effects were observed for the experimental 2-butanol dehydration barriers [12]. For Keggin-type POM clusters and various mineral acids, weaker acids (with higher DPE values) typically form anionic clusters with a higher charge density, often as a consequence of their smaller size and larger number of protons, and these anionic species effectively stabilize cations and lead to more negative ΔE_{int} values [12]. The observation that ΔE_{int} values become more negative as the number of charge-balancing protons increases (e.g. $H_3PW_{12}O_{40}$, ΔE_{int} = 318 kJ mol^{-1}; $H_5AlW_{12}O_{40}$, ΔE_{int} = 335 kJ mol^{-1}) for acids of identical anion size can be understood by considering the charge of the anionic conjugate base as $H^{\delta+}_{8-n}(X^{n+}W_{12}O_{40})^{(1+(8-n)\delta)-}$. This shows that the electron density in the $X^{n+}W_{12}O_{40}$ conjugate base increases with decreasing valence of X and that the electrostatic stabilization of cations becomes stronger as the number of charge-balancing protons concurrently increases.

The compensation found between ΔE_{int} and DPE reflects the nature of DPE values as the energy cost for charge separation

to form the non-interacting proton and anionic conjugate base. Weaker acids (with larger DPE values) require a large energy input for charge separation, but this energy is recovered in part by the interactions of the resulting anion with other cations (as transition states or intermediates). The distance between anionic clusters and cations is smallest for the proton removed in the process described by DPE, because protons lack core electrons and their repulsive effects. Thus, DPE values can only be *partially* compensated by ΔE_{int} upon formation of the ion pairs at transition states [19].

For 2-butanol dehydration on Keggin-type POM clusters, DFT calculations have shown that ΔH_{ads} values (see also Scheme 2, Step 1) changed from -77 kJ mol^{-1} ($H_3PW_{12}O_{40}$) to -73 kJ mol^{-1} ($H_5AlW_{12}O_{40}$) as DPE values and barriers increased by 34 kJ mol^{-1} and 13.4 kJ mol^{-1}, respectively [14]. Similar weak correlations between DPE and ΔH_{ads} are expected in general for Brønsted acids, because alkanol adsorption involves hydrogen-bonding interactions between protons and oxygen atoms in alkanols; these interactions are ubiquitous for other Brønsted acids. This suggests that the effect of composition on rate constants and activation barriers for alkanol dehydration reactions predominantly reflects the stabilization of cationic transition states and, therefore, the effects of DPE, instead of differences in the stability of adsorbed precursors on sites with different DPE values.

Reliable DPE estimates are unavailable from theory for SZr, WZr, and SAR catalysts because of the uncertain structure of their acid sites. 2-Butanol dehydration rate constants on SZr, WZr, and SAR are indicated by horizontal lines at their respective values in the ordinate of Fig. 3. This line intersects that defined by elimination rate constants on POM clusters and zeolites at a value corresponding to the DPE values for SZr, WZr, and SAR catalysts.

In this manner, we can rigorously estimate a value for the acid strength of these materials, specifically at the conditions in which they operate as catalysts and as a specific quantity. These values rank a broad range of solid acids in terms of experimentally elusive acid strengths; they also provide a method to benchmark the fidelity of various structures suggested for acid sites in SZr, WZr, and SAR solids by comparing these DPE values with those calculated for these hypothetical site structures. The DPE estimates are 1165 kJ mol^{-1}, 1185 kJ mol^{-1}, and 1154 kJ mol^{-1} for SZr, WZr, and SAR. SZr and SAR are similar in acid strength, but slightly stronger than zeolites and weaker than Keggin-type POM clusters. The acid strength of WZr resembles that for sites in H-BEA at the conditions of alkanol dehydration catalysis. DPE values for Keggin POM and H-BEA represented in Eq. (2) correspond to sites with uniform structure. A distribution of sites (and DPE values), possible for SZr, WZr, and SAR, makes the DPE values reported here the reactivity-weighed averages that are consequential for their catalytic behavior.

These DPE estimates assume that the extent to which ΔE_{int} compensates DPE terms, as reflected by Eq. (2) and the data shown in Fig. 3 for materials of known structure, is also applicable to SZr, WZr, and SAR. We consider this to be a reasonable assumption. ΔE_{int} estimates calculated for the stabilization of Na^+ cations by the deprotonated anionic conjugate base for several acids with DPE values ranging from 1080 kJ mol^{-1} ($HC_5(CN)_5$) to 1480 kJ mol^{-1} (HF) gave ΔE_{int} values of -397 kJ mol^{-1} to -643 kJ mol^{-1}; these values showed a maximum deviation of ±15 kJ mol^{-1} from the ΔE_{int} estimated by the best linear fit of ΔE_{int} as a function of DPE (see supporting information for calculated values of DPE and ΔE_{int}). These deviations provide an upper bound for the expected deviations of the DPE estimates for SZr, WZr and SAR from true values, because SZr, WZr, and SAR all contain oxo-type species, as in the case of the POM clusters and zeolites from which ΔE_{int}–DPE correlations were established.

3.4. Kinetics and mechanism for n-hexane isomerization on SO_4–ZrO_2 and WO_x–ZrO_2

Elementary rate constants for isomerization steps can only be accurately measured when *n*-hexane isomerization occurs on bifunctional catalysts containing a metal function used to maintain hydrogenation–dehydrogenation equilibrium [51]. Monofunctional alkane isomerization on Brønsted acids is limited by initiation steps that involve protolytic alkane dehydrogenation, instead of isomerization steps. These dehydrogenation steps may also be catalyzed by redox sites, provided either by the solid acid (or by spurious impurities) and are unrelated to acid chemistry, and often require temperatures that degrade the inorganic acid or deplete the sites or the spurious impurities [38,39]. SZr and WZr catalysts dehydrogenate alkanes via stoichiometric reduction processes of SO_x and WO_x species, respectively, a property often misinterpreted as evidence for very strong acid sites [38,39]. Thus, monofunctional alkane isomerization reactions on SZr and WZr are controlled by their ability to form alkenes via catalytic or stoichiometric redox processes that do not depend on the strength of their Brønsted acid sites. The presence of metal function, in contrast, provides constant and known alkene concentrations along the catalyst bed.

Fig. 4 shows *n*-hexane isomerization turnover rates (per accessible proton titrated by 2,6-di-*tert*-butylpyridine; Table 1) on physical mixtures of SZr (Fig. 4a) or WZr (Fig. 4b) with Pt/Al_2O_3 (Pt/H^+ = 1) as a function of the (nC_6/H_2) molar ratio in the inlet stream. Reaction rates increased with increasing (nC_6/H_2) molar ratios, linearly at first and then more gradually, on both SZr and WZr catalysts, as also observed on POM and H-BEA catalysts [19] (Fig. 4a and b). Varying H_2 or nC_6 pressures at constant (nC_6/H_2) molar ratios did not influence isomerization turnover rates. These data are consistent with quasi-equilibrated dehydrogenation–hydrogenation equilibrium and with the catalytic sequence discussed next.

Quasi-equilibrated hydrogenation–dehydrogenation steps on the Pt function and elementary steps involved in the isomerization of the resulting alkenes on Brønsted acid sites are depicted in Scheme 3. Dehydrogenation forms equilibrated mixtures of linear hexene isomers (Scheme 3, Step 1), which are protonated on Brønsted acid sites to form the corresponding alkoxides (Scheme 3, Step 2). The position of the double bond in *n*-hexene isomers is kinetically-irrelevant because hydride shifts within alkoxide intermediates are fast and quasi-equilibrated. Alkoxides isomerize via protonated dialkylcyclopropane transition states [17] to form monobranched isomers (Scheme 3, Step 3), which deprotonate to form isoalkenes (Scheme 3, Step 4) that hydrogenate on Pt (Scheme 3, Step 5) to complete the bifunctional isomerization cycle. At (sufficiently) high Pt/H^+ ratios, dehydrogenation occurs reversibly and much more rapidly than isomerization; therefore, alkene and isoalkene concentrations remain in equilibrium with their respective alkanes. On the sample with the highest volumetric *n*-hexane isomerization rate (H_3PW/SiO_2; 0.04 POM nm^{-2}), isomerization rates became independent of Pt content for Pt/H^+ ratios above ~0.2; [19] thus, equilibrium is certain at the Pt/H^+ ratios of unity used here. Co-impregnated Pt/$H_{8-n}X^{n+}W/SiO_2$ samples and physical mixtures of H_3PW/SiO_2 with Pt/Al_2O_3 gave identical isomerization rate constants, thus ruling out artifacts caused by intrapellet alkene gradients [19].

The assumptions of alkane dehydrogenation (Scheme 3, Steps 1 and 5) and alkene protonation/alkoxide deprotonation equilibria (Scheme 3, Steps 2 and 4) are consistent with data [19,21] and DFT calculations [17]. Irreversible and kinetically-relevant alkoxide isomerization steps (Scheme 3, Step 3) give the rate equation:

$$r_{isom} = \frac{k_{isom} K_{prot} K_{dehy} \frac{[nC_6]}{[H_2]} [H^+]}{1 + K_{prot} K_{dehy} \frac{[nC_6]}{[H_2]}} \quad (3)$$

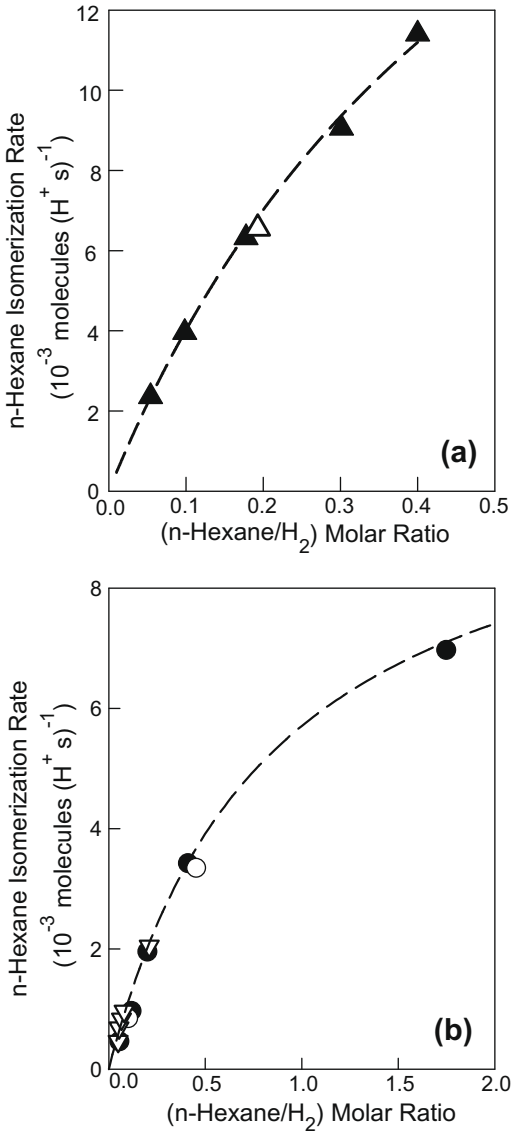

Fig. 4. *n*-Hexane isomerization rates (per accessible H^+) as a function of (nC_6/H_2) for a physical mixture of (a) SZr and Pt/Al_2O_3 (473 K, $Pt/H^+ = 1$, 30 kPa H_2 (▲), 60 kPa H_2 (Δ) or (b) WZr and Pt/Al_2O_3 (473 K, $Pt/H^+ = 1$, 30 kPa H_2 (●), 60 kPa H_2 (○), 80 kPa H_2 (▽)). The dashed lines represent fits to the rate data using Eq. (3).

Table 1
2,6-Di-*tert*-butylpyridine uptake measured by titration during 2-butanol dehydration (0.2 kPa 2-butanol, 0.9 Pa 2,6-di-*tert*-butylpyridine) and *n*-hexane isomerization reaction (473 K, 0.2 (nC_6/H_2), 1.4 Pa 2,6-di-*tert*-butylpyridine) (Figs. 2 and 6).

	2,6-Di-*tert*-butylpyridine uptake during	
	2-Butanol dehydration	*n*-Hexane isomerization
SZr	0.16 (S-atom)$^{-1}$	0.28 (S-atom)$^{-1}$
WZr	0.06 (W-atom)$^{-1}$	0.05 (W-atom)$^{-1}$
SAR	1.00 (H^+)$^{-1}$	Not measured

which also accurately describes rate data also on Keggin-type POM clusters [19] and zeolites [40]. In Eq. (3), k_{isom} is the isomerization rate constant (Scheme 3, Step 3), K_{prot} is the equilibrium constant for *n*-alkoxide formation (Scheme 3, Step 2), K_{dehy} is the dehydrogenation equilibrium constant (Scheme 3, Step 1), and [H^+] is the concentration of protons accessible during catalysis, reported here from titration of acid sites by 2,6-di-*tert*-butylpyridine. Values for k_{isom} and K_{prot} were determined by regressing rate data to the form of Eq. (3), while K_{dehy} was obtained from thermodynamic data [41].

Fig. 4 shows *n*-hexane isomerization rates predicted from Eq. (3) using values for k_{isom} and K_{prot} obtained by regressing rate data to the form of Eq. (3) for SZr (Fig. 4a) and WZr (Fig. 4b) (dashed curves). The excellent agreement between predicted and measured rates (Fig. 4) confirms the accuracy of Eq. (3) in describing *n*-hexane isomerization rates on SZr and WZr. SAR showed a very different kinetic behavior, which we address at the end of this section.

Hydrogen transfer from alkanes to alkoxides, required to desorb the latter as alkanes, can propagate carbenium ion cycles without requiring alkane dehydrogenation on SZr [25]. These hydride transfer steps would lead to isomerization rates proportional to alkane concentrations and independent of H_2 pressures, in contradiction with the linear dependence on (nC_6/H_2) ratios observed and predicted from Eq. (3). This kinetic dependence reflects the fact that alkanes (instead of alkenes) determine surface hexoxide concentrations. Thus, we conclude that hydride transfer pathways are inconsequential at the conditions of our measurements.

Brønsted acid sites form on WZr via stoichiometric reduction of WO_x domains with concomitant formation of acidic O-H groups [31,42,43]. The formation of these temporary acid sites via reductive processes led to a first-order dependence of *o*-xylene isomerization rates on H_2 pressure, even though H_2 is not required (mechanistically or stoichiometrically) for *o*-xylene isomerization turnovers [43]. The different kinetic dependences on H_2 pressures for *o*-xylene isomerization (first-order) and *n*-hexane isomerization ($\sim(nC_6/H_2)$) reflect the essential absence of unsaturated species during isomerization catalysis (<1 Pa hexenes); such unsaturated hydrocarbons act as oxidants by scavenging hydrogen from surfaces, thus reversing stoichiometric reduction steps that form Brønsted acid sites. The higher oxidant concentrations (~1 kPa) prevalent during *o*-xylene isomerization remove hydrogen atoms more rapidly and thus require H_2 activation to control the number of Brønsted acid sites during steady-state catalysis. A more detailed discussion of the effects of oxidant/reductant concentrations on the number of temporary Brønsted acid sites is included in the supporting information section.

n-Hexane isomerization rates cannot be described by Eq. (3) on sulfonic acid resins (SAR). The (nC_6/H_2) ratios used on SZr and WZr catalysts (0.05–1; Fig. 4) did not give detectable isomerization rates on SAR at 473 K. The use of pure *n*-hexane reactants, however, led to detectable formation of isohexanes. Fig. 5a shows *n*-hexane isomerization rates as a function of equilibrium *n*-hexene pressures (combined for all *n*-hexene isomers) on SAR and SZr. Above ~35 Pa *n*-hexenes pressures, *n*-hexane isomerization rates resembled those measured on SZr at much lower pressures (~0.04 Pa). Isomerization rates increased with increasing *n*-hexene concentrations on SAR, first linearly and then more gradually. In contrast with SZr, which deactivates at *n*-hexene pressures above ~0.1 Pa (Fig. 5b), because of the high prevalent alkoxide concentrations and concomitant oligomerization side reactions, SAR catalysts did not deactivate even at hexene pressures >35 Pa.

SAR catalysts consist of agglomerates of polymeric persulfonic acid resins and colloidal SiO_2 particles, a morphology that differs markedly from that in inorganic solids, such as POM clusters, zeolites, SZr, and WZr. The protons within perfluorosulfonic acid resin particles cannot be reached by non-polar species [33], but become accessible when polar reactants, such as alkanols and ethers, expand the resin structures, as shown by the similar kinetic behavior of SAR, SZr, and WZr materials in the case of 2-butanol dehydration reactions (Fig. 1). The restricted access of hexenes (and hexanes) causes intraparticle concentration gradients and low local hexane and hexene concentrations. These lead, in turn, to low isomerization rates, but also to even larger effects on the rates of bimolecular oligomerization reactions (Fig. 5b).

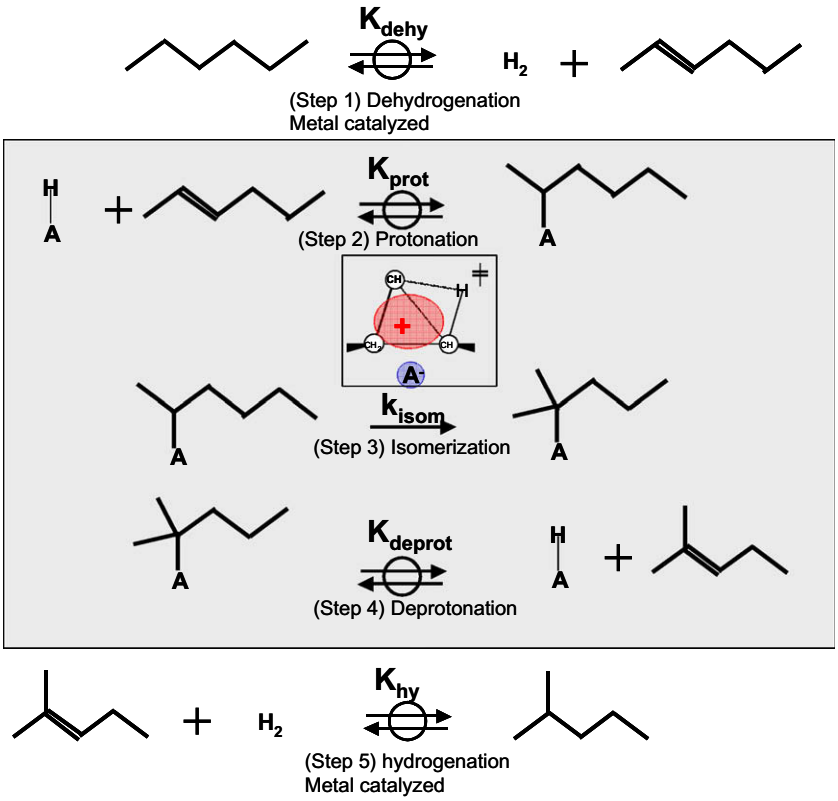

Scheme 3. Proposed sequence of elementary steps for *n*-hexane isomerization on bifunctional metal–Brønsted acid catalysts [19].

3.5. Measurement of the number of accessible protons during n-hexane isomerization by 2,6-di-tert-butylpyridine titration on SO_4–ZrO_2 and WO_x–ZrO_2

Fig. 6 shows *n*-hexane isomerization turnover rates as Brønsted acid sites were titrated by 2,6-di-*tert*-butylpyridine on SZr–Pt/Al_2O_3 mixtures. The left panel in Fig. 6 shows *n*-hexane isomerization rates before introducing the titrants, while the right panel shows rates as a function of the amount of titrant adsorbed. *n*-Hexane isomerization rates decreased linearly as 2,6-di-*tert*-butylpyridine titrated Brønsted acid sites (Fig. 6). The titrant uptake required to suppress isomerization rates was 0.28 per S-atom in the sample (Fig. 6 and Table 1). 2,6-di-*tert*-Butylpyridine titrations on WZr also led to a linear decrease and to the complete suppression of isomerization rates. The measured titrant uptake required to suppress isomerization rates was 0.05 per W-atom in WZr (Table 1).

The amount of titrant required to titrate all sites on SZr was slightly larger during *n*-hexane isomerization (0.28 S-atom^{-1}, Fig. 6) than during 2-butanol dehydration (0.16 S-atom^{-1}, Fig. 2). These results may seem surprising at first, because water has been implicated in the conversion of Lewis acids into Brønsted acid sites on these materials; [44] thus, we expect a higher density of Brønsted acid sites during 2-butanol dehydration (~10–20 Pa H_2O formed) than in the anhydrous environment prevalent during isomerization catalysis. It is possible that any Brønsted acid sites formed by H_2O interactions with Lewis acid sites are too weak to bind 2,6-di-*tert*-butylpyridine irreversibly and to catalyze 2-butanol dehydration. DPE estimates derived from 2-butanol dehydration rate constants are higher (and acid sites are thus weaker) than those derived from hexane isomerization rate constants (see Section 3.7 for data and detailed discussion). Thus, we conclude that the reaction environment influences the number and strength of acid sites and, by inference, their local structure.

In contrast, titrant uptakes required to suppress reaction rates on WZr were smaller during *n*-hexane isomerization ($0.05H^+WO_x^{-1}$, Table 1) than during 2-butanol dehydration ($0.06H^+$ W-atom^{-1}, Table 1). These data appear to reflect OH recombination events, which remove Brønsted acid sites and occur more readily at the higher temperatures (473 K vs. 343 K for 2-butanol dehydration) and anhydrous conditions of isomerization catalysis. These reaction-dependent titrant uptakes on WZr and SZr illustrate the essential requirement that the number of accessible Brønsted acid sites be measured *during* reaction and that theoretical treatments consider hypothetical structures consistent with these effects of reaction environment on the structure of acid sites.

3.6. Deprotonation energy estimates from n-hexane isomerization rate constants for SO_4–ZrO_2 and WO_x–ZrO_2

Fig. 7 shows measured *n*-hexane isomerization rate constants (in a log scale) on Keggin-type POM clusters supported on SiO_2 ($H_{8-n}X^{n+}W_{12}O_{40}$, $X = P^{5+}$, Si^{4+}, Al^{3+}, Co^{2+}; in order of increasing DPE) and on H-BEA zeolite as a function of their DPE values (calculated from DFT). As in the case of 2-butanol dehydration reactions, the line through the data suggests a common exponential dependence of isomerization rate constants on DPE [19], as expected from the thermochemical cycle formalism in Section 3.3. *n*-Hexane isomerization rate constants on SZr and WZr are shown as horizontal lines defined by their measured rate constants at the ordinate, because their uncertain structures make theoretical DPE estimates unreliable. The intersection of these lines with that regressed through the data on POM and zeolite catalysts of known structure allows DPE to be estimated for SZr and WZr at the conditions of isomerization catalysis. These DPE values are 1110 kJ mol^{-1} for SZr and 1120 kJ mol^{-1} for WZr, indicating that SZr and WZr are stronger acids than zeolites and similar in strength to the weakest POM acids ($H_6CoW_{12}O_{40}$ and $H_5AlW_{12}O_{40}$; Table 2). These DPE

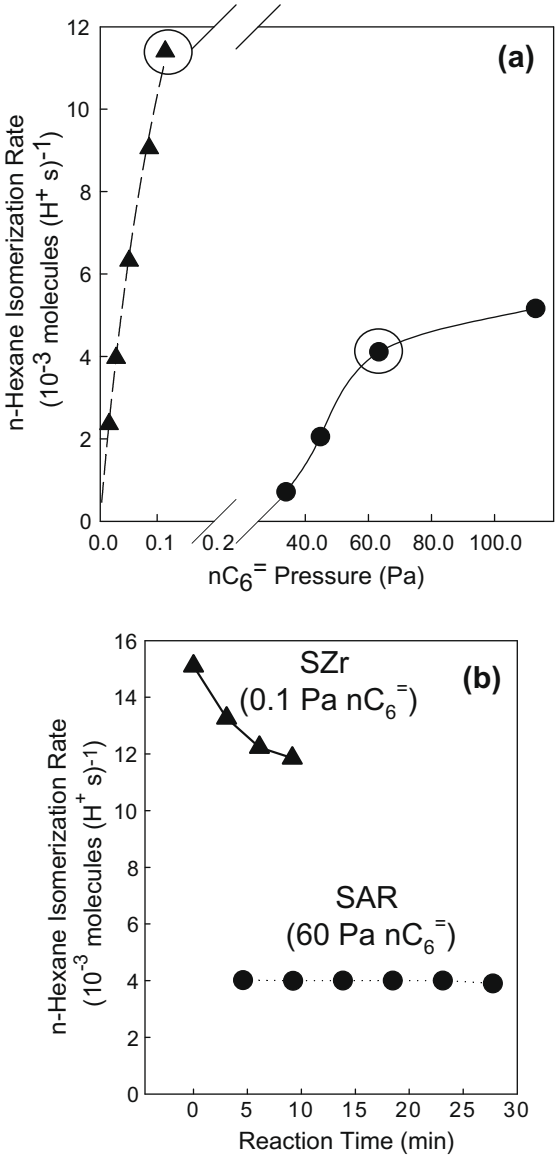

Fig. 5. (a) *n*-Hexane isomerization rates (per H^+) as a function of n $C_6^=$ (*n*-hexene) pressure on physical mixtures of SAR (●) or SZr (▲) and Pt/Al_2O_3 mixtures (473 K, $Pt/H^+ = 1$). The dashed line represents a fit to the rate data using Eq. (3). (b) *n*-Hexane isomerization rates on SAR (●) (~60 Pa $nC_6^=$) or SZr and Pt/Al_2O_3 mixtures (▲) (~0.1 Pa $nC_6^=$) as a function of reaction time. $nC_6^=$ pressures were calculated from nC_6 (and H_2 pressures) at reaction temperatures assuming (de)hydrogenation equilibrium.

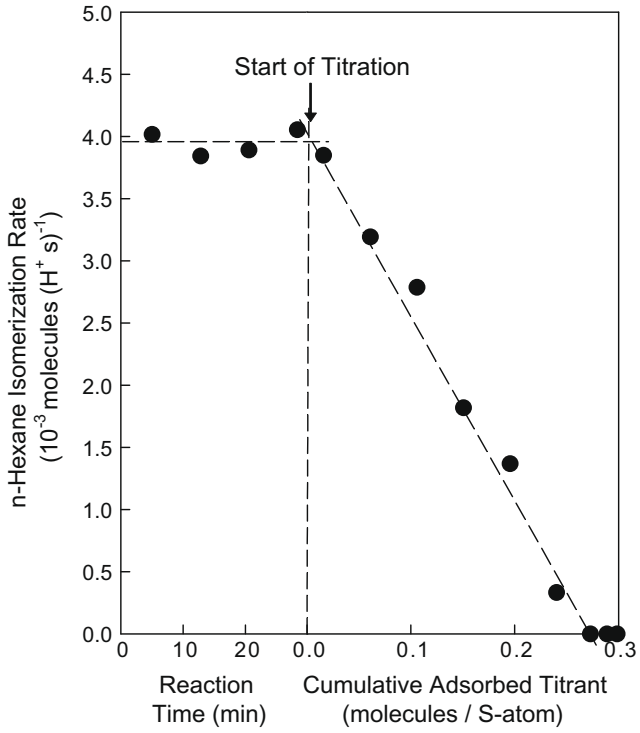

Fig. 6. Titration of acid sites for a physical mixture of SZr and Pt/Al_2O_3 during *n*-hexane isomerization at 473 K. Reaction rates (per H^+) as a function of the cumulative amount of titrant (2,6-di-*tert*-butylpyridine) adsorbed (473 K, 0.2 (nC_6/H_2), 1.4 Pa 2,6-di-*tert*-butylpyridine).

values differ somewhat from those obtained from 2-butanol dehydration rate constants on WZr and SZr (Section 3.3). Next, we interpret these differences in DPE values in terms of plausible effects of treatment or reaction conditions on the identity and strength of Brønsted acid sites. These effects, taken together with DPE estimates, provide useful benchmarks for possible structures of Brønsted acid sites at conditions imposed by specific catalytic reactions.

3.7. Implications of DPE values and of their dependence on reaction condition for the nature of Brønsted acid sites on SO_4–ZrO_2 and WO_x–ZrO_2

The DPE estimates of 1165 kJ mol^{-1} (SZr) and 1185 kJ mol^{-1} (WZr) obtained from 2-butanol dehydration rate constants are larger than those determined from isomerization rate constants (1110 kJ mol^{-1} for SZr and 1120 kJ mol^{-1} for WZr) (Table 2). Such differences in DPE values are significant and of the same magnitude as the entire range of DPE values covered by the POM compositions examined (56 kJ mol^{-1} range; 1087 kJ mol^{-1} to 1143 kJ mol^{-1} for $H_{8-n}X^{n+}W_{12}O_{40}$, with X = P, Si, Al, Co). These reaction-dependent DPE values may reflect inaccurate data or inappropriate assumptions in our approach, neither of which are evident from our data or from their analysis. They may reflect instead effects of reaction environment or treatment conditions, which differ between elimination and isomerization catalysis, on the number, structure, and strength of Brønsted acid sites.

One assumption in our method for estimating DPE for unknown structures is that the ΔH_{ads} terms (Eq. (2)) for SZr, WZr, and SAR depend on DPE either weakly for all materials or in the same manner as in the case of Keggin clusters and H-BEA samples, on which the reactivity-DPE relations in Figs. 3 and 7 are based. For example, different extents of reactant stabilization by various acids, reflected in the ΔH_{ads} term in Eq. (2), could lead to different DPE estimates from *n*-hexane isomerization and 2-butanol dehydration reactions (Eq. (2)). Hexoxide intermediates, with significant covalent character, may respond to catalyst composition or structure more sensitively than the H-bonded butanol species involved in dehydration reactions. The K_{prot} values for SZr and WZr (4.4 Pa^{-1} and 3.1 Pa^{-1}, respectively) are smaller than those for POM clusters with similar acid strength (8.9 Pa^{-1}, $H_5AlW_{12}O_{40}$) and those for H-BEA (21.9 Pa^{-1}) (Table 3). These data show that the stability of covalently-bound alkoxides is not related to the acid DPE [19]. DFT calculations showed that the stability of H-bonded alkanol reactants (interacting with H-atoms in the acid) decreased only slightly with increasing DPE for POM clusters [14]. On both POM clusters and H-BEA, covalent *n*-hexoxide species became slightly more stable with increasing DPE (Table 3) [19]. These weak effects indicate that the different sensitivities of 2-butanol dehydration and hexane isom-

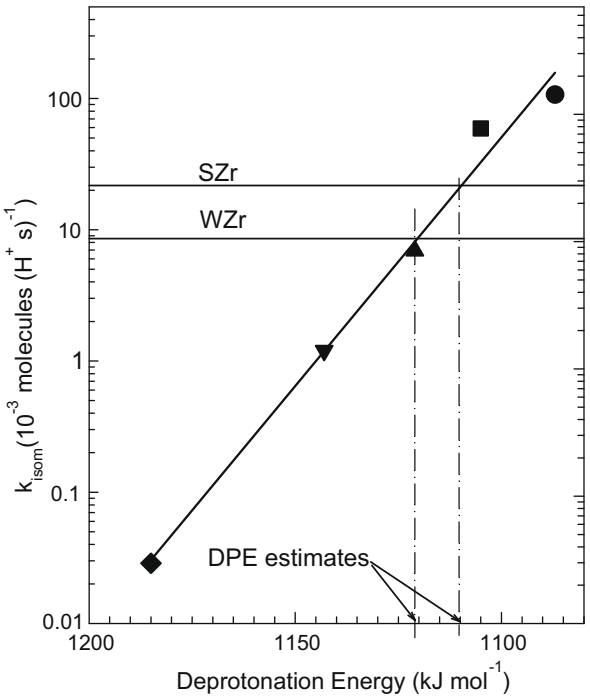

Fig. 7. *n*-Hexane isomerization (k_{isom}) (Scheme 3, Step 3) rate constants as a function of deprotonation energy (ΔE_{rxn} for HA → A^- + H^+(non-interacting), where HA is the acid and A^- is the conjugate base) calculated by DFT for physical mixtures of Pt/Al_2O_3 (473 K, Pt/H^+ = 1) and 0.04H_3PW/Si (●), 0.04H_4SiW/Si (■), 0.04H_5AlW/Si (▲), 0.04H_6CoW/Si (▼), and H-BEA (◆) Measured *n*-hexane isomerization rate constants on SZr and WZr are shown as solid horizontal lines. k_{isom} values where obtained by fitting Eq. (3) to the kinetic data and normalization by the 2,6-di-*tert*-butylpyridine uptake, which corresponds to the number of accessible protons.

erization to DPE do not arise from different effects of DPE on adsorbed reactants as a result of their different charge.

We can exclude any significant role of DPE in reactant stability even more convincingly by examining the dependence of the $k_{isom}K_{prot}$ product (instead of k_{isom}) on DPE for known acid structures. The value of $k_{isom}K_{prot}$ depends only on the enthalpy and entropy of transition states relative to gas-phase hexenes and does not include any contributions from the energetics of adsorbed hexoxides. These $k_{isom}K_{prot}$ data (Table 2; see also $k_{isom}K_{prot}$ vs. DPE figure in supporting information) give DPE values of 1112 kJ mol^{-1} and 1130 kJ mol^{-1} for SZr and WZr, respectively; these are the same as those obtained from k_{isom} on SZr and ~10 kJ mol^{-1} higher on WZr (Table 2). DPE estimates from $k_{isom}K_{prot}$, which do not depend on the stability of adsorbed intermediates, remain much smaller (~55 kJ mol^{-1}) for isomerization than for elimination on both WZr and SZr. We conclude, therefore, that DPE effects on reactant stability are not responsible for the differences in DPE values derived from isomerization and dehydration rate data on both

Table 2
DPE estimates from 2-butanol dehydration and *n*-hexane isomerization rate constants (from measured data and correlations between reactivity and DPE in Figs. 3 and 7).

	Deprotonation energy values (kJ mol^{-1})		
	2-Butanol dehydration	*n*-Hexane isomerization	
	from k_2	from k_{isom}	from $k_{isom}K_{prot}$
SZr	1165	1110	1112
WZr	1185	1120	1130
SAR	1154		

Table 3
DPE values or estimates and equilibrium constants for alkoxide formation (K_{prot}) (Scheme 3, Step 2).

	DPE (kJ mol^{-1})	K_{prot} (Pa^{-1})
$H_3PW_{12}O_{40}$	1087	4.1[a]
$H_5AlW_{12}O_{40}$	1121	8.9[a]
H-BEA	1185	21.9[a]
SZr	1110[b]	4.4
WZr	1120[b]	3.1

[a] See Ref. [19].
[b] See also Table 2.

SZr and WZr. We discuss next, first for WZr and then for SZr, other possible causes of reaction-dependent DPE values.

On WZr, DPE values are smaller during *n*-hexane isomerization than during 2-butanol dehydration catalysis. These differences may reflect some dehydroxylation, resulting from the anhydrous environment and the higher temperatures prevalent in isomerization catalysis. Dehydroxylation is known to increase acid strength (decrease DPE) for residual protons in POM clusters, because of a concomitant decrease in the charge density of the anionic conjugate base as the number of protons decreases [14]. This leads to a decrease in the energy required for charge separation because of the greater stability of the anion, as discussed in Section 3.3. Dehydroxylation of $H_3PMo_{12}O_{40}$ (to $HPMo_{12}O_{39}$) and of reduced $H_5PMo_{12}O_{40}$ (to $H_3PMo_{12}O_{39}$) clusters decreased DPE values by ~16 kJ mol^{-1} in each case [14]. Partial dehydroxylation is consistent with the smaller number of protons measured by 2,6-di-*tert*-butylpyridine during isomerization than during dehydration catalysis (0.05 vs. 0.06H^+ W-$atom^{-1}$; Table 1).

On SZr, DPE values were 55 kJ mol^{-1} smaller from *n*-hexane isomerization than from 2-butanol dehydration rate data, suggesting that, as in the case of WZr, SZr is a stronger acid under the anhydrous conditions of isomerization catalysis. *n*-Hexane isomerization rates increased ~50-fold when SZr catalysts were treated in He at 673 K before reaction (the procedure used for the data shown in Figs. 4–7) than when treated in He only at 473 K. The isomerization rate constant measured on SZr samples treated at 473 K, when placed on the regressed line in Fig. 7, leads to a DPE estimate of 1157 kJ mol^{-1}, which is 47 kJ mol^{-1} larger than on the SZr sample treated at 673 K (1110 kJ mol^{-1}). In fact, this DPE estimate for the sample treated at 473 K is very similar to that obtained on SZr during 2-butanol dehydration at 343 K (1165 kJ mol^{-1}). We note that 2-butanol dehydration rate constants were unaffected by thermal treatment before reaction (673 K for 2 h vs. untreated), apparently because the extent of hydroxylation (and the acid strength) is established by the alkanol dehydration environment itself. The conditions during alkanol dehydration favor more hydroxylated surfaces and weaker acid sites than the anhydrous conditions of isomerization reactions. DFT calculations show that H_2O adsorbs weakly even on strongly acidic $H_3PW_{12}O_{40}$ clusters (ΔH_{ads} = −67.5 kJ mol^{-1}) [35]. Thus, thermal treatments are not likely to increase acid strength by merely causing water desorption. These strong effects of thermal treatment and reaction environment on hydroxylation and acid strength indicate that estimates of acid strength remain equivocal in value, and perhaps even kinetically-inconsequential, except when measured *during* catalysis. We conclude that the removal of OH groups by thermal treatment at 673 K leads to stronger Brønsted acid sites, which are preserved during anhydrous alkane isomerization; OH groups can re-form, however, during dehydration reactions of protic reactants, such as alkanols.

We discuss next how interactions of H_2SO_4 species with molecules such as H_2O and SO_3 (relevant to Brønsted acid sites in SZr) influence their DPE value. Similar interactions may give rise to

the observed effects of pretreatment on rates and to the differences in DPE values derived from alkanol dehydration and alkane isomerization rate data (Table 2).

DPE values derived from 2-butanol dehydration and *n*-hexane isomerization rate constants on SZr (1165 kJ mol^{-1}, 1110 kJ mol^{-1}, respectively) are smaller than for isolated gas-phase H_2SO_4 monomers (1293 kJ mol^{-1}). Two types of interactions among H_2SO_4, H_2O, and SO_3 decrease DPE values for H_2SO_4 monomers. Cooperativity effects decrease DPE by forming $(H_2SO_4)_2$ dimers (1220 kJ mol^{-1} vs. 1293 kJ mol^{-1} for H_2SO_4) (Scheme 4a), in which the deprotonated anion is stabilized by another H_2SO_4 molecule via H-bonding. Strong effects of H_2O molecules on acid strength for liquid H_2SO_4–H_2O mixtures are also well-known [45]. The DPE of H_2SO_4 monomers decreases also upon formation of Brønsted–Lewis conjugate acids, such as in complexes consisting of a H_2SO_4 monomer interacting with one ($H_2S_2O_7$, Scheme 4b) or two ($H_2S_3O_{10}$, Scheme 4b) SO_3 molecules, which act as Lewis acids:

$$H_2SO_4 + nSO_3 \leftrightarrow H_2S_{n+1}O_{4+3n} \quad (4)$$

These Brønsted–Lewis acid pairs give DPE values of 1177 kJ mol^{-1} for $H_2S_2O_7^{46}$ and 1127 kJ mol^{-1} for $H_2S_3O_{10}^{46}$ (cf. 1293 kJ mol^{-1} for H_2SO_4 monomers [46]). More effective electron delocalization over larger anionic clusters, caused by association or complexation of H_2SO_4 monomers, increases acid strength, either via cooperativity effects or via the formation of Brønsted–Lewis conjugate acids. H_2O, in contrast, decomposes $(H_2SO_4)_2$ dimers and Brønsted–Lewis acid pairs and leads to an increase in the electron density at anionic clusters, thus decreasing acid strength.

The effects of cooperativity (−73 kJ mol^{-1}) and Brønsted–Lewis complexation (−115 kJ mol^{-1}) on DPE are stronger for H_2SO_4 monomers than the effects of reaction environment on 2-butanol dehydration and *n*-hexane isomerization on DPE reported here (−55 kJ mol^{-1}). Treatment at high temperatures and anhydrous conditions favor Brønsted–Lewis conjugate acids via dehydroxylation, which forms SO_3-like species from sulfonic acid groups in SZr. In contrast, protic species, such as alkanols and water, coordinate to Lewis centers and disrupt Brønsted–Lewis acid pairs, via reactions analogous to:

$$H_2S_2O_7 + H_2O \rightarrow 2H_2SO_4 \quad (5)$$

which increases the number of Brønsted acid sites but also their DPE values (from 1177 kJ mol^{-1} for $H_2S_2O_7^{46}$ to 1293 kJ mol^{-1} for H_2SO_4 monomers [46]). These trends are consistent with the stronger acids found in SZr at the anhydrous conditions of alkane isomerization than when butanol is present in dehydration reactions. These conclusions provide an interpretation for the thermal treatments required to detect catalytic reactivity in SZr samples. Thermal treatments cause dehydroxylation and a consequent increase in the acid strength of residual OH groups via cooperativity effects as SO_x groups form and interact with sulfonic acid groups (instead of water) (Scheme 4a). Dehydroxylation can also form Brønsted–Lewis conjugate acids via condensation (analogous to the reverse of Eq. (4)) or decomposition of H_2SO_4 to SO_3, which interacts with sulfonic acid groups to form grafted analogs of strongly acidic $H_2S_2O_7$ species (Eq. (4)) (Scheme 4b).

Cooperativity effects and reversible formation of Brønsted–Lewis acid pairs are possible only for weakly-bound SO_x species, which can interact with Lewis acids (e.g. SO_3) to decrease DPE or with Lewis bases (e.g. H_2O) to increase DPE. Active acid sites in SZr may resemble those in supported phosphoric acid catalysts, for which P-NMR [31] indicate that species that interact with basic probe molecules consist of H_3PO_4monomers and $H_3PO_4(PO_3)_n$ oligomers [47]. Silicon phosphate species with strong support interactions were unaffected by these molecules because they do not act as Brønsted acids [47]. Similarly, species resembling H_2SO_4 monomers and $H_2SO_4(SO_3)_n$ oligomers, instead of SO_x species strongly bound on ZrO_2, may act as the active acid sites on SZr, consistent with the strong effects of pre-treatment and reaction conditions and with the arguments proposed here to explain these effects.

Some sulfate groups in SZr (~40%) can be removed by contact with liquid water at 298 K, indicating that they interact weakly with ZrO_2 surfaces [25]. Such SO_x can react with SO_3 or H_2O to form or consume Brønsted–Lewis conjugate acids. The formation of such Brønsted–Lewis conjugate acids was proposed to account for the weakening of antisymmetric S–O stretches in oligomeric SO_x species with increasing H_2O concentration, as a result of hydrolysis of S–O–S bonds and decomposition of Brønsted–Lewis conjugate acids [48].

We conclude that the strengthening of acid sites via Brønsted-acid/Lewis-acid complexation upon dehydroxylation and their weakening by interactions with Lewis bases account for the effects of reaction environments on DPE values for WZr. Anhydrous isomerization conditions give lower DPE values (1120 kJ mol^{-1}, Table 2) than those prevailing during dehydration reactions (1185 kJ mol^{-1}, Table 2) because the extent of dehydroxylation differs in these two reaction environments.

Rate constants for *n*-hexane isomerization and 2-butanol dehydration on SZr indicate that DPE values (1120 and 1165 kJ mol^{-1}) are significantly smaller than for H_2SO_4 monomers (1293 kJ mol^{-1}) or $(H_2SO_4)_2$ dimers (1220 kJ mol^{-1}), but lie between those calculated for H_2SO_4–SO_3 (1177 kJ mol^{-1}) and H_2SO_4–$(SO_3)_2$ complexes (1127 kJ mol^{-1}) in the gas phase. Our DPE estimates are significantly smaller than those reported from theoretical estimates for hypothetical SZr structures at various SO_3 and H_2O pressures (1353–1499 kJ mol^{-1}), which are also larger than for H_2SO_4 monomers [49]. These previous studies have suggested that SZr contains active sites consisting of pyrosulfate anions ($S_2O_7^{2-}$) bound in a tridentate configuration on ZrO_2 with two vicinal bridging hydroxyl

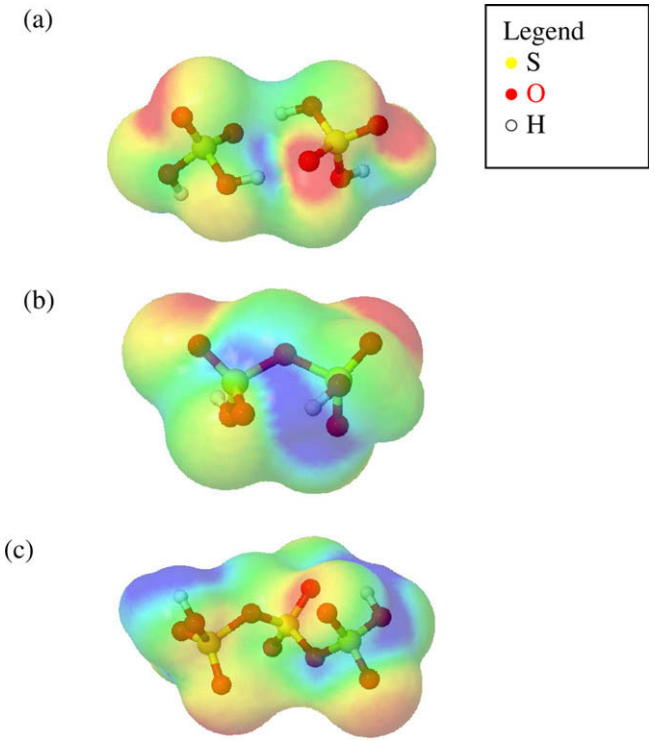

Scheme 4. H_2SO_4 dimer (cooperativity effect) (a), Brønsted–Lewis conjugate acids $H_2S_2O_7$ (b) and $H_2S_3O_{10}$ (c). The colored surfaces correspond to the van der Waals surfaces of the molecules. The color scheme shows whether areas on these surfaces are electropositive (blue) or negative (red).

groups on ZrO_2 support and one adsorbed water molecule [49]. In this structure, the protons are associated with ZrO_2 and not with the SO_x moiety and are very weakly acidic (1418 kJ mol^{-1} DPE) [49,50]. These DPE values derived from DFT for SZr [49,50] would lead to undetectable isomerization rates according the correlations shown in Fig. 7. Thus, we conclude that such species may indeed represent the most stable structures, but their stability and strong interactions with ZrO_2 render them essentially unreactive and inconsequential in Brønsted acid catalysis by SZr.

DPE estimates from the *n*-hexane isomerization and 2-butanol dehydration rate constants indicate that the identity of the active Brønsted acid sites of SZr is sensitive to reaction conditions and to treatment protocols. Their acid strength is determined by the extent to which Brønsted–Lewis conjugate acid-type interactions occur as the extent of dehydroxylation evolves in catalytic environments.

We have shown here that the acid strength can be assessed in terms of quantitative values for deprotonation energies for Brønsted acids with unknown site structures from the dynamics of catalytic reactions. This approach requires mechanistic interpretations of measured rates, knowledge about the number of acid sites present during catalysis, and a correlation between rate constants for the kinetically-relevant elementary steps and deprotonation energies derived from data on solid acids with known structure. The method proposed is not specific to any catalyst or reaction. It probes acid strength at the prevailing reaction conditions from the stability of cationic transition states, accessible through thermochemical cycles and consequential to catalysis on solid acids. These DPE estimates provide a rigorous benchmark to assess the fidelity of structures proposed for acid sites in these materials and a method to probe how such structures depend on reaction environments.

4. Conclusions

DPE values for solid acids of unknown structure have been estimated by comparing their measured rate constants to previously developed rigorous correlations between rate constants and DPE on Keggin-type POM and H-BEA. This method is possible because the structures of POM clusters and acid zeolites are known, allowing their DPE values to be calculated by DFT. We have demonstrated this approach by measuring turnover rates on SZr, WZr, and SAR for 2-butanol dehydration and *n*-hexane isomerization, which are interpreted as kinetic rate constants by independent measurements of acid site density by chemical titration using 2,6 di-*tert*-butylpyridine. Although these provide specific examples, this technique can be widely applied to any reaction whose kinetically-relevant step is catalyzed by Brønsted acid sites. The kinetics of 2-butanol dehydration on SZr, WZr, and SAR catalysts and of *n*-hexane isomerization on SZr or WZr as physical mixtures with Pt/Al_2O_3 were identical to those obtained for Keggin-type POM clusters and H-BEA catalysts, allowing for their interpretation as kinetic rate constants. Physical mixtures of SAR with Pt/Al_2O_3, however, exhibited a low reactivity in *n*-hexane isomerization, presumably because of its low Brønsted-acid site accessibility in non-polar environments. The deprotonation energy (DPE) values estimated using the measured rate constants and the correlations established earlier for Keggin-type POM clusters and zeolite H-BEA are 1110 kJ mol^{-1} and 1120 kJ mol^{-1} for SZr and WZr, respectively, based on the *n*-hexane isomerization rate constants, and 1165 kJ mol^{-1}, 1185 kJ mol^{-1} and 1154 kJ mol^{-1} for SZr, WZr and SAR, based on their 2-butanol dehydration rate constants. From these estimates, we conclude acid sites on SZr and SAR are stronger than those found in acid zeolites, but are weaker than those found on $H_3PW_{12}O_{40}$ and $H_4SiW_{12}O_{40}$ Keggin clusters. Depending on its reaction environment, WZr acid sites are either stronger (*n*-hexane isomerization) or nearly equal (2-butanol dehydration) to those of acid zeolites. For SZr and WZr, lower DPE estimates during *n*-hexane isomerization relative to 2-butanol dehydration demonstrate the subtle effects of reaction environment on catalytic acid sites and the importance of utilizing methods that measure acid strength at catalytically relevant conditions.

Acknowledgments

Support by the Chemical Sciences, Geosciences, Biosciences Division, Office of Basic Energy Sciences, Office of Science US Department of Energy under grant number DE-FG02-03ER15479 is gratefully acknowledged. We thank Professors Matthew Neurock and Michael Janik (University of Virginia) for their contributions to the theory that underpinned our study, Dr. Cindy Yin (UC-Berkeley) for the synthesis of bulk H_5A1W and H_6CoW clusters, and Professor Johannes Lercher from the Technical University of Munich, Professor Chelsey Baertsch, and Ms. Cathy Chin for the SZr, WZr and Pt/Al_2O_3 catalysts.

Appendix A. Supplementary data

Supplementary data associated with this article can be found, in the online version, at doi:10.1016/j.jcat.2009.03.005.

References

[1] A. Corma, Chem. Rev. 95 (1995) 559, and references therein.
[2] A. Zecchina, F. Geobaldo, G. Spoto, S. Bordiga, G. Ricchiardi, R. Buzzoni, G. Petrini, J. Phys. Chem. 100 (1996) 16584.
[3] A. Zecchina, S. Bordiga, G. Spoto, D. Scarano, G. Spano, F. Geobaldo, J. Chem. Soc., Faraday Trans. 92 (1996) 4863.
[4] C. Paze, S. Bordiga, C. Lamberti, M. Salvalaggio, A. Zecchina, G. Bellussi, J. Phys. Chem. B 101 (1997) 4724.
[5] F. Haase, J. Sauer, J. Phys. Chem. 98 (1994) 3083.
[6] M. Hunger, Catal. Rev. – Sci. Eng. 398 (1997) 345.
[7] J.F. Haw, T. Xu, Adv. Catal. 42 (1998) 115.
[8] C. Paze, S. Bordiga, A. Zecchina, Langmuir (2000) 8139.
[9] R. Buzzoni, S. Bordiga, G. Ricchinardi, G. Spoto, A. Zecchina, J. Phys. Chem. 99 (1995) 11937.
[10] W.E. Farneth, R.J. Gorte, Chem. Rev. Chem. Rev. 95 (1995) 615.
[11] N. Mizuno, M. Misono, Chem. Rev. 98 (1998) 199.
[12] J. Macht, M.J. Janik, M. Neurock, E. Iglesia, J. Am. Chem. Soc. 130 (2008) 10369.
[13] J. Macht, M.J. Janik, M. Neurock, E. Iglesia, Angew. Chem., Int. Ed. 46 (2007) 7864.
[14] M.J. Janik, J. Macht, E. Iglesia, M. Neurock, J. Phys. Chem. C 113 (2009) 1872.
[15] M. Boronat, P. Viruela, A. Corma, J. Phys. Chem. A 102 (1998) 982.
[16] V.B. Kazansky, Catal. Today 51 (1999) 419.
[17] T. Demuth, X. Rozanska, L. Benco, J. Hafner, R.A. van Santen, H. Toulhoat, J. Catal. 214 (2003) 68.
[18] M.J. Janik, R.J. Davis, M. Neurock, Catal. Today 116 (2006) 90.
[19] J. Macht, R.T. Carr, E. Iglesia, J. Am. Chem. Soc., in press.
[20] P.B. Weisz, in: D.D. Eley, P.W. Selwood, P.B. Weisz (Eds.), Advances in Catalysis and Related Subjects, vol. 13, Academic Press, New York, 1962, p. 137.
[21] F.J.M.M. de Gauw, J. van Grondelle, R.A. van Santen, J. Catal. 206 (2002) 295.
[22] M. Hino, K. Arata, Chem. Commun. (1980) 851.
[23] E. Iglesia, S.L. Soled, G.M. Kramer, J. Catal. 144 (1993) 238.
[24] X. Song, A. Sayari, Catal. Rev. – Sci. Eng. 38 (1996) 329.
[25] X. Li, K. Nagaoka, L.J. Simon, R. Olindo, J.A. Lercher, J. Catal. 232 (2005) 456.
[26] K. Arata, M. Hino, in: M.H. Phillips, M. Ternan (Eds.), Proceedings of the 9th International Congress on Catalysis, The Chemical Institute of Canada, Ottawa, 1988, p. 1727.
[27] E. Iglesia, D.G. Barton, S.L. Soled, S. Miseo, J.E. Baumgartner, W.G. Gates, G.A. Fuentes, G.D. Meitzner, in: J.W. Hightower, W.N. Delgass, E. Iglesia, A.T. Bell (Eds.), Proceedings 11th International Congress of Catalysis Stud. Surf. Sci. Catal., vol. 101, Elsevier, Amsterdam, 1996, p. 533.
[28] J.G. Santiesteban, J.C. Vartuli, S. Han, R.D. Bastian, C.D. Chang, J. Catal. 168 (1997) 431.
[29] M.A. Harmer, W.E. Farneth, Q. Sun, J. Am. Chem. Soc. 118 (1996) 7708.
[30] C. Morterra, G. Cerrato, C. Emanuel, V. Bolis, J. Catal. 142 (1993) 349.
[31] C.D. Baertsch, K.T. Komala, Y.-H. Chua, E. Iglesia, J. Catal. 205 (2002) 44.
[32] X. Li, K. Nagaoka, J.A. Lercher, J. Catal. 227 (2004) 130.
[33] Q. Sun, W.E. Farneth, M.A. Harmer, J. Catal. 164 (1996) 62.
[34] M.J. Frisch et al., Gaussian 03, revision C.02, Gaussian Inc., Wallingford, CT, 2004.

[35] M.J. Janik, K.A. Campbell, B.B. Bardin, R.J. Davis, M. Neurock, Appl. Catal. A 56 (2003) 51.
[36] D. Farcaşiu, R. Leu, A. Corma, J. Phys. Chem. B 106 (2002) 928.
[37] M.T. Aronson, R.J. Gorte, W.E. Farneth, J. Catal. 98 (1986) 434.
[38] X.B. Li, K. Nagaoka, L.J. Simon, R. Olindo, J.A. Lercher, A. Hofmann, J. Sauer, J. Am. Chem. Soc. 127 (2005) 16159.
[39] S. Kuba, P.C. Heydorn, R.K. Grasselli, B.C. Gates, M. Che, H. Knözinger, Phys. Chem. Chem. Phys. 3 (2001) 146.
[40] A. van de Rundstraat, J.A. Kamp, P.J. Stobbelaar, J. van Grondelle, S. Krijnen, R.A. van Santen, J. Catal. 171 (1997) 77.
[41] D.R. Stull, E.F. Westrum, G.C. Sinke, The Chemical Thermodynamics of Organic Compounds, Robert E. Krieger Publishing Company, Malabar, 1987.
[42] D.G. Barton, S.L. Soled, G.D. Meitzner, G.A. Fuentes, E. Iglesia, J. Catal. 181 (1999) 57.
[43] R.D. Wilson, D.G. Barton, C.D. Baertsch, E. Iglesia, J. Catal. 194 (2000) 175.
[44] J.F. Haw, J. Zhang, K. Shimizu, T.N. Venkatraman, D.-P. Luigi, W. Song, D.H. Barich, J.B. Nicholas, J. Am. Chem. Soc. 122 (2000) 12561.
[45] V.B. Kazansky, Catal. Today 73 (2002) 12.
[46] I.A. Koppel, P. Burk, I. Koppel, I. Leito, T. Sonoda, M. Mishima, J. Am. Chem. Soc. 122 (2000) 5114.
[47] T.R. Krawietz, P. Lin, K.E. Lotterhos, P.D. Torres, D.H. Barich, A. Clearfield, J.F. Haw, J. Am. Chem. Soc. 120 (1998) 8502.
[48] C. Morterra, G. Cerrato, F. Pinna, M. Signoretto, G. Strukul, J. Catal. 139 (1994) 181.
[49] C. Breitkopf, H. Papp, X. Li, R. Olindo, J.A. Lercher, R. Lloyd, S. Wrabetz, F.C. Jentoft, K. Meinel, S. Förster, K.M. Schindler, H. Neddermeyer, W. Widdra, A. Hofmann, J. Sauer, Phys. Chem. Chem. Phys. 9 (2007) 3600.
[50] A. Hofmann, J. Sauer, J. Phys. Chem. B 108 (2004) 14652.
[51] P.B. Weisz, E.W. Swegler, Science 126 (1957) 31.
[52] R. Thorton, B.C. Gates, J. Catal. 34 (1974) 275.